Effects of compositional proportions, metal-ion concentration and pH conditions into the structural characteristics of Au, Pt and AuPt nanoparticles

R. Esparza, J.A. Ascencio, and R. Pérez*
Instituto de Ciencias Físicas, Universidad Nacional Autónoma de México,
P.O. Box 48-3, Cuernavaca, Mor., 62251, México,
Phone: +52 (55) 5622 7797, Fax: +52 (55) 5622 7770,
∗e-mail: ramiro@fis.unam.mx

G. Rosas
Instituto de Investigaciones Metalúrgicas, Universidad Michoacana de San Nicolás de Hidalgo,
P.O. Box 52-B, Morelia, Mich., 58000, México.

U. Pal
Instituto de Física, Universidad Autónoma de Puebla,
Apartado Postal J-48, Puebla, Pue., 72570, México.

Nanometric metallic particles of Pt, Au and Au/Pt of different nominal compositions were synthesized using a chemical reduction method with a polymer (PVP) as the protecting agent. The effects of the gold ion concentrations and also of the concentration of the reducing agent compound, on the morphology and structural characteristics of the obtained gold nanoparticles have been explored. Particles with different pH reaction mixtures have been synthesized. High resolution transmission electron microscopy (HRTEM) observations have been used in the nanoparticles characterization. Depending of the pH reaction mixtures, different nanometric sizes and consequently different atomic structural configurations of the particles are obtained. Theoretical simulations based on molecular dynamics have been used to interpret some of the experimental results and also to get an insight on macroscopic properties such as: stability and catalytic activity.

Keywords: Platinum; gold; nanostructures; metallic particles; bimetallic particles; chemical synthesis; characterization; electron microscopy; electronic structure.

Partículas metálicas nanométricas de Pt, Au y Au/Pt de diferente composición nominal fueron sintetizadas usando el método de reducción química utilizando un polímero (PVP) como agente protector. Los efectos de la concentración de los iones de oro y del agente reductor han sido explorados en la morfología y en las características estructurales de las nanopartículas de oro. Se han sintetizado nanopartículas con diferentes pH finales de reacción. Microscopía electrónica de alta resolución ha sido usada en la caracterización de las nanopartículas. Dependiendo del pH final de reacción, diferentes tamaños nanométricos y consecuentemente diferentes configuraciones estructurales de las partículas son obtenidas. Simulaciones teóricas basadas en dinámica molecular han sido usadas para interpretar algunos de los resultados experimentales y para tener una perspectiva de las propiedades macroscópicas tales como: estabilidad y actividad catalítica.

Descriptores: Platino; oro; nanoestructuras; partículas metálicas; partículas bimetálicas; síntesis química; caracterización; microscopía electrónica; estructura electrónica.

PACS: 61.46.Df; 81.07.Bc; 81.16.Be; 68.37.Og

1. Introduction

Nanoparticles are defined as atomic arrangements with nanometric dimensions and usually with a small number of constituent atoms. The control of the size and the dispersion of nanometric metal particles have an important effect on their physical properties [1,2]. The dispersion of small metallic particles in polymeric membranes has been widely used in new technological applications [3,4]. Nanoparticles and other nanostructures have been obtained recently using different synthesis methods [5-7]. In this investigation we report the experimental results on the synthesis of nanoparticles using a chemical reducing method [3]. The selection of the chemical procedures of this reduction method can give rise to particular structural configurations of particles [8,9]. Therefore, the variations of concentration of the main reagent

compound and also the variations of the reduction agent are explored in relation with the morphological and structural characteristics of the synthesized nanoparticles. On the other hand, Pt nanoparticles are one of the best catalysts for fuel cells. Although impressive progress has been made on the synthesis of platinum nanoparticles, the majority of the work was focused on the investigation of Pt clusters with a diameter less than 20 nm [10]. However, gold nanoparticles have received great interests due to their attractive electronic, optical, and thermal properties as well as catalytic properties and potential applications in the fields of physics, chemistry, biology, medicine, and materials science and their different interdisciplinary fields [11], and therefore, the synthesis and characterization of gold nanoparticles have attracted considerable attention from a fundamental and practical point of

view [12]. Bimetallic gold and platinum nanoparticles have been described at various occasions; they are of interest because of their special catalytic properties [13]. The structural determination of the nanoparticles becomes an important task to understand some of their properties [14,4]. The use of the TEM and associated methods has been established as one of the main tools in the study of nanomaterials [15,16]. Also, a complete understanding of the atomic distribution and the corresponding effects on the electronic, chemical and optical properties also requires theoretical methods based on molecular dynamic theories [16,17]. Some of the structural characterizations of the nanometric metallic particles have been obtained through comparisons between experimental and theoretical HRTEM images [18,19]. In this study, the morphology and structural characteristics of nanoparticles of Pt, Au and Pt/Au in the range of 1-10 nm are obtained. These nanoparticles were synthesized through a chemical reduction method with manipulation of synthesis conditions in order to recognize the optimal parameters to control size and structure.

2. Experimental procedure

The synthesis of nanostructured materials is one of the main research topics in the nanoscience scientific and technological community. Thus, for example, chemical methods have been commonly used for the synthesis of nanoparticles, nanotubes and nanorods. The experimental results presented in this communication have been obtained using the chemical reduction method. In the chemical reduction approach, solutions of methanol of Au or Pt ions were prepared by dissolving the corresponding crystallites in methanol, crystalline hydrogen tetrachloroaurate ($HAuCl_4.xH_2O$) or hydrate hydrogen hexachloroplatinate ($H_2PtCl_6.6H_2O$). Both solutions ($HAuCl_4.xH_2O$ and $H_2PtCl_6.6H_2O$) were mixed in desired volumetric ratios for the preparation of bimetallic ion mixtures. In all the samples, the total ion concentration in the reacting solutions was kept fixed (0.066 mmol in 100 ml). In the gold case, different concentrations of the reagent compounds ($HAuCl_4.xH_2O$) have been used. The concentrations include: 0.033, 0.044, 0.099 and finally 0.12 mmol in 25 ml of methanol. A methanol solution of PVP [poly (N-vinil-2-pyrrolidone)], based on 150 mg of PVP with molecular weight of 40,000 in 50 ml of methanol, was added to the metal ions. An aqueous solution of $NaBH_4$ (0.066 M) was added to the mixture solution at room temperature to reduce the metal ions. A homogeneous colloidal dispersion was formed after the addition of $NaBH_4$ reductor in the solution containing metal ions. Another aspect of interest in this reduction approach is the effect of the concentration of the reducing agent on the size and morphology of the small metallic particles. Therefore, in the gold case, two fixed concentration of the reagent compound ($HAuCl_4.xH_2O$) of 0.014 and 0.066 mmol in 25 ml of methanol was used with different concentrations of the reducing agent (final pH values 4 and 7).

The structural and morphological characteristics of the dispersed nanoparticles have been studied using a Philips Tecnai F20 transmission electron microscope with accelerating voltage of 200 kV with a point resolution of ≈2.1 Å. TEM specimens were prepared by dispersing and subsequent drying a drop of colloidal solutions on a copper grid (3 mm in diameter) covered with an amorphous carbon film. Theoretical simulations based on classical molecular dynamics were also performed. We used quantum mechanics calculations based in the density functional theory (DFT). These calculations were performed using the DMol3 software of Accelrys [20] considering a Perdew-Wang functional (PW91) [21].

3. Results and discussion

3.1. Pt, Au and Au/Pt nanoparticles

The synthesis of the nanoparticles induces a surface energy reduction that generates the boundaries and the minimal energy structures. However, when they are immersed in a polymeric matrix, the size and the surface effects in the cluster shape become more important. Although, normally the pre-synthesized nanoparticles are being incorporated in the polymeric matrix for their modification, the analysis of the particles encapsulated in polymer matrix may present a better way to understand the size distribution and the structural effects on the dispersion and properties changes of the membrane. The use of variations on concentration of metal ions besides the pH effects is evaluated here and firstly we show the basis for the analysis. In order to determine the effect of particular concentration (0.033 mmol) and pH (pH=7) condition on the capability of producing small nanoparticles even for different elements and bimetallic arrays is shown here and studied deeply in a previous work [22,23].

Figure 1a shows a low magnification transmission electron microscopy (TEM) image of Pt particles encapsulated by PVP; the size of these nanoparticles can be measured directly from the TEM image with help of selected area and contour determination as it is shown from Fig. 1a (region i) [22,24]. This technique was using to measure the particle size in all the synthesized nanoparticles. The particle size distributions for PVP capped nanoparticles of Pt, Au, Au/Pt (1:1), and Au/Pt (3:1) are illustrated in Fig. 1b. The sample population was 500 particles. It can be seen that while for pure Pt, the average particle size is 2.11 nm with small dispersion in size, for pure Au, the average particle size is 1.78 nm, and the size dispersion is even less. The size distributions for the Au/Pt (1:1) and Au/Pt (3:1) colloidal particles reveal average particle sizes of 2.06 nm and 1.82 nm, respectively. It is interesting to note that even when the Au/Pt (1:1) sample reveals a larger average particle size, there are still about 15% smaller particles (<1 nm) in the sample. Both the bimetallic samples show size dispersions higher than those of the pure elemental cases. The size of the obtained nanoparticles denotes the range where quantum effects are present. However, at this size scale the shape and structure generate important changes in the chemical potential and the reactivity [22,23].
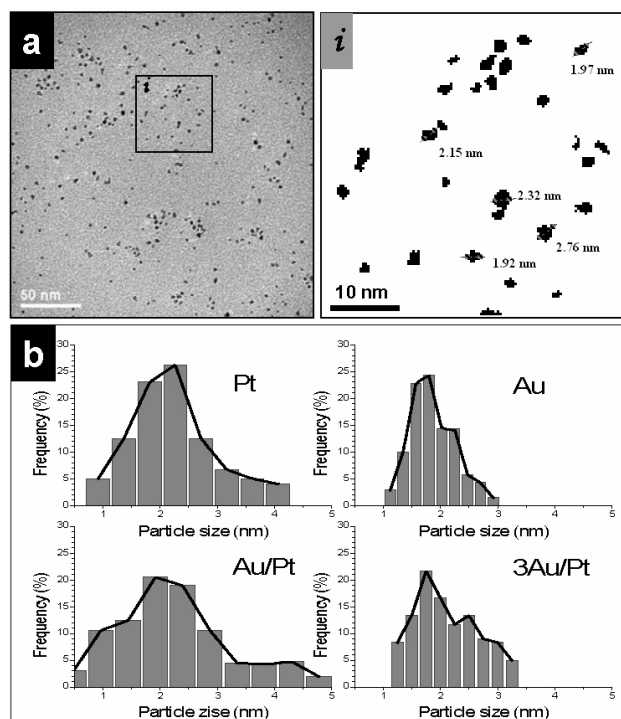
FIGURE 1. Low magnification transmission electron microscopy analysis of samples with different compositions (Pt, Au and Au/Pt). a) Common image and b) size distribution plot.
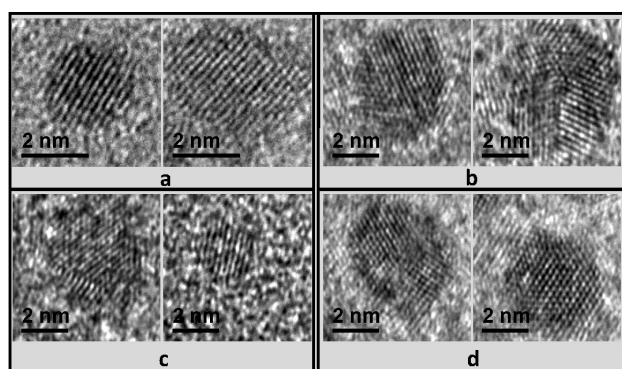
FIGURE 2. HRTEM images of samples with different compositions. a) Pt, b) Au, c) Au/Pt 1:1 and d) Au/Pt 3:1 proportions.

In order to determine the structures of the nanoparticles, HRTEM images from the particles of different sizes have been studied. Figure 2 shows the HRTEM images obtained from the different samples. So then, first image of Pt clusters (Fig. 2a) match to a cubic (fcc-like) particle in the [123] orientation, where linear fringes are well-identified; while the second image can be associated to a similar particle structure, but in this case the lattice fringes are slightly deformed and it corresponds to a rotation of the electron beam near to the [011] orientation [25,16]. The HRTEM images obtained from the nanometric particles of gold (Fig. 2b) show an fcc-like cluster slightly rotated from the [011] direction; and a multiple twin particle, which can be associated to the truncated decahedron in an orientation near to five fold [26,27].

These images show that some of the nanometric Au particles display the presence of twin boundaries which were not seen in the Pt particles.

Twin boundaries are also observed for Au/Pt particles containing different concentrations of Au as it can be observed in their corresponding HRTEM images. By instance, micrographs of Fig. 2c, from samples of Au/Pt (1:1), show multiple twinned structures. Besides nanometric particles with composition Au/Pt (3:1) show different types of structures as it is illustrated in Fig. 2d, determining them as a single twinned particle and a deformed metallic particle respectively for the selected images.

The structural morphology of the nanometric metallic particles is strongly dependent on the stiochiometry as it is illustrated in Fig. 3, where the frequency of the structural shapes as a function of nominal composition is displayed. In the figure, cubic (fcc-like), cubic with deformation (fccd), decahedral (deca), other multiple twin particles (mtp), single twin particles (stp), and highly deformed particles (hdp) are the main structural configurations of the clusters. The Pt particles show fcc-like structural morphologies only. However, the Au particles have fcc like and decahedron-like shapes. The Au/Pt (1:1) sample shows fcc-like and multiple twinned particles and finally the Au/Pt (3:1) composition shows decahedron-like and also twinned particles. Such structural evolutions involve multiple factors and the most important is related to the surface energy minimization, which is clearly higher for the pure Pt. In fact the existence of twin clusters for the nanoparticles implies an internal strain, which is released by means of the defects [15].

In order to understand the effects of the energy in the formation of a specific configuration, we performed the geometry optimization of the clusters. In Table I, the binding energies for the different calculated models are shown, basically with examples of decahedral and cubooctahedral structures for pure metal clusters, Pt shell over an Au core (Pt/Au). A configuration of parallel twined structure, where the elements
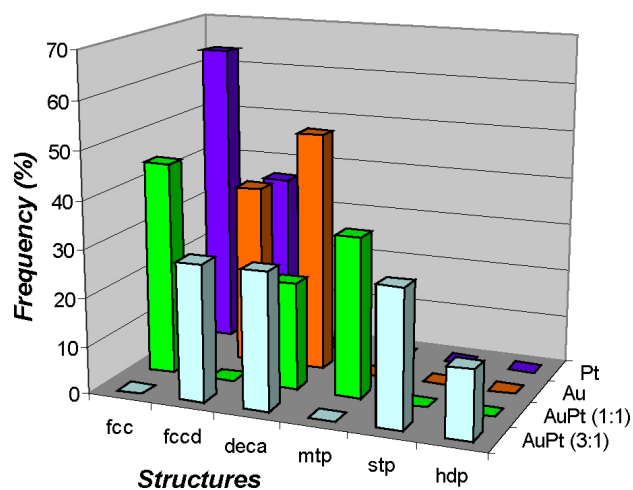
FIGURE 3. Structure distribution plot for the different composition samples.

TABLE I. Energy analysis for the different structural and compositional configurations.

Structure	Configuration	Pt atoms	Au atoms	Binding Energy (eV)	Coherence Energy (eV)	Gap. (eV)
Cubo-	Pt	55	0	-269.721	0.000	0.050
Octahedral	Au	0	55	-139.965	0.000	0.354
	PtAuAlloy	31	24	-215.023	-1.923	0.099
	PtAuAlloy	24	31	-201.416	-4.831	0.151
	Pt shell /Au core	42	13	-251.551	-12.499	0.168
	Pt core/ Au shell	13	42	-177.381	-6.745	0.155
Decahedral	PtAuAlloy	35	20	-236.156	-2.895	0.231
	PtAuAlloy	20	35	-177.554	-6.919	0.219
	Pt shell/Au core	42	13	-223.203	-0.666	0.091
	Pt core/Au shell	13	42	-193.713	-6.564	0.123
Parallel	Au/Pt/Au	27	28	-207.491	-3.828	0.008
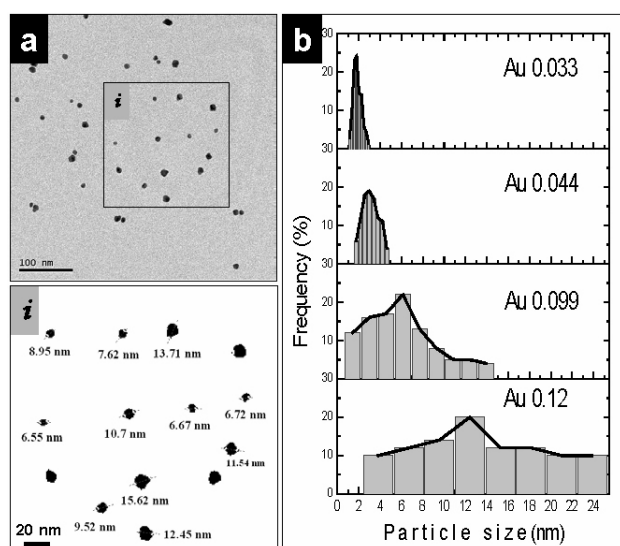
FIGURE 4. Low magnification transmission electron microscopy analysis of samples with different metal-ion concentrations. a) Common image and b) size distribution plot.

are arranged (Au/Pt/Au), is also included in order to understand the effect of this kind of defect and to compare its stability of a few observed clusters in the produced samples. Beside the total binding energy, we considered the coherence energy that relates the contribution of each type of atom and the corresponding energy of formation of the pure elemental clusters. From the binding energy values, it is clear that the lowest energy structure is the pure Pt cluster; however, considering the coherency component, the most stable configuration is the Pt/Au cubooctahedron. From these values, it is clear that the presence of higher proportion of Pt atoms in the bimetallic clusters favors fcc-like structures, and a higher concentration of Au atoms generates both fcc-like and decahedron structures. In fact, the different configurations are nearly stable and they must coexist in the samples, with a preference for fcc-like structures for the particles with higher

number of Pt atoms; whereas, the Pt shell around Au core with the cubooctahedral shape is the most stable structure, where the 42 Pt atoms are covering the 13 atoms of the Au core. Also in table we can find the energy gap between the highest occupied molecular orbital (HOMO) and the lowest unoccupied molecular orbital (LUMO) for each of the modeled structures.

We can observe that when the number of Pt atoms increases, the corresponding conductivity increases too, and it is clear that the density of electrons on the particle surface increases similarly. It is interesting to note that for the parallel twined structure, the conductivity is increased significantly, up to 6 times that of obtained for pure Pt. From the calculated chemical potential values [28], we can identify the most stable structure as the Au-core/Pt shell; however, the energy difference between the structures is quite small for the pure Au and the bimetallic clusters. This characteristic is the basis for the multiple configurations obtained in the samples. The corresponding electronic structure for the different configurations establishes the feasibility of having enough electrophilic and nucleophilic sites in the polymer membrane when the clusters are incorporated [29,30].

3.2. Au nanoparticles synthesized by different metal-ion concentration

One of the main parameters to evaluate efficiency of the methods is to increase the amount of material to produce nanoparticles; however, its use is critical in the selection of parameters, because the saturation of the solution can generate bigger clusters up to bulk structures. In our case, we decided to test different values of metal-ion concentrations (0.033, 0.044, 0.099 and 0.12 mmol of $HAuCl_4.xH_2O$) to identify the effects on the size and the structure of the produced clusters. Small Au nanoparticles have been obtained using the chemical reduction method previously described for all the considered concentrations, however significant dif-

ferences are recognized. Figure 4 shows an analysis of the particles produced by different concentrations, including a low magnification electron microscope image of a sample produced with 0.099 mmol of Au (Fig. 4a), with its corresponding contour determination of a selected area (region i) that illustrate the method to determine the size of the synthesized particles and the size distribution plot for all the samples (Fig. 4b). The average size particle is displayed as a function of the reagent compound concentration. These average sizes range from less than 2 nm for 0.033 mmol samples to approximately 12 nm for the 0.12 mmol concentration sample.

The nature of the atomic structural configurations is also strongly dependent on the reagent compound concentration. Thus, for example, for the different concentrations, Fig. 5 shows the most commonly found configurations. For 0.033 mmol it is shown a fcc-like particles besides a truncated decahedron structure (Fig. 5a), while for a concentration of 0.044 it can be determined the presence of single twined particles and fcc-like ones (Fig. 5b). Samples produced at
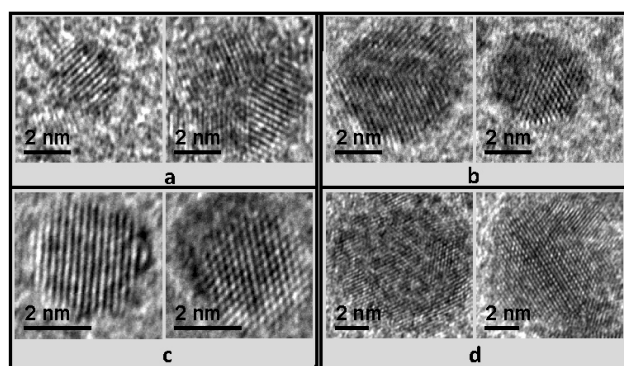
FIGURE 5. HRTEM images of samples with different metal-ion concentrations; nanoparticles produced with a) 0.033, b) 0.044, c) 0.099 and d) 0.12 mmol (of $HA_uCl_{4.x}H_2O$).
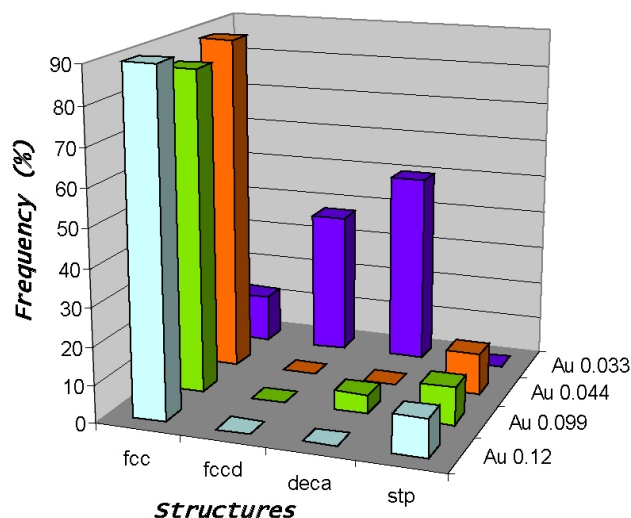
FIGURE 6. Structure distribution plot for the different metal-ion concentration samples.

0.099 mmol induce mainly fcc-like clusters with well ordered arrays (Fig. 5c), similarly to the observed for 0.12 mmol, where the contrast is mainly of lines and locally periodic dots (Fig. 5d).

A statistical summary of these atomic structural characteristics are illustrated in Fig. 6. At low concentrations of the reagent compound (0.033), the more commonly found structures are decahedra and fcc-deformed, however, as soon as, the concentration is increased (0.044, 0.099 and 0.12), the most commonly found structures change to single twinned particles and fcc-like particles. It is also important to mention that the particle sizes for the low concentrations are also the smallest obtained with this synthesis reduction method, only a few nanometers in size and in average less than 2 nanometers. Therefore, depending on the concentration of the reagent compound, two main regions of different atomic structural particle characteristics can be found. Low concentrations (0.033) induced the formation of decahedra and fcc-deformed gold particles. However, higher concentrations (0.044, 0.099 and 0.11 mmol) induced the formation of single twinned particles and fcc-like particles. A qualitative insight of the atomic structural characteristics of the gold nanometric particles can be obtained using the consideration about the effect of the surface energy in the production of the clusters atomistic structure, which determines that the lowest energy configurations tend to generate multiple twinned particles, and when the particles increase their size and energy they tend to form crystal bulk type of structure [31,32].

3.3. Structural and morphological characteristics of gold nanoparticles as a function of the pH (Concentration of reducing agent "NaBH$_4$").

Based on the previous mentioned results, and looking to identify the extreme parameters that induce a controlled size on the particles following the reported method, we determine to reduce the concentration of metal ions in the synthesis. The observed evidences of this reduction of ion concentration were evaluated at two different pH conditions in order to determine the possibility to recognize the effect of the reduction agent, besides the consequently proton saturation of the solution. So, with the purpose of controlling the particle sizes and the particles structure, HAuCl$_4$.xH$_2$O with different concentrations of the reducing agent NaBH$_4$ has been studied, which chemically determines the pH conditions and consequently the amount of protons in the solution during the synthesis. We considered two different metal-ion concentrations for the synthesis of the nanoparticles in order to evaluate the extremes that our previous results denoted. In both cases, pH values were controlled to be 4 and 7, generating a comparative analysis.

From Fig. 7, an example of the evaluated micrographs is shown; in this case, the image corresponds to a sample obtained with a concentration of 0.014 mmol and a pH=4, which shows particles from 4.5 up to 10.3 nm approximately
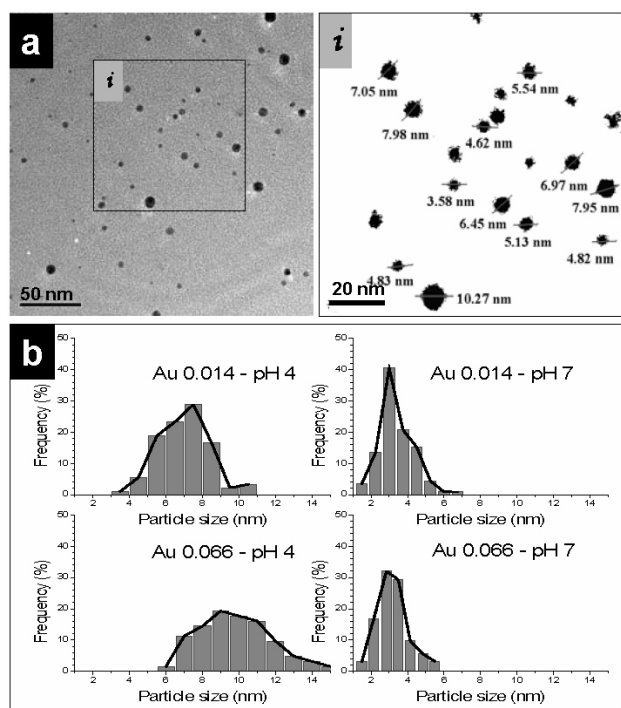
FIGURE 7. Low magnification transmission electron microscopy analysis of samples with different variation of metal ion concentration and pH. a) Standard TEM image and b) size distribution plot.
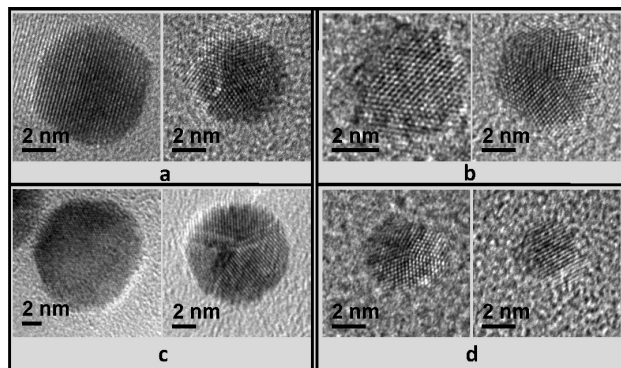
FIGURE 8. HRTEM images of nanoparticles obtained under different synthesis conditions. Concentration of 0.014 mmol with pH a) 4 and b) 7; besides concentration of 0.066 mmol with pH c) 4 and d) 7.

(see region *i*). The size distribution plot of Fig. 7b denotes significant differences when the samples are obtained at pH=4 and pH=7. While samples generated at pH=7 follow a similar tendency than that reported in the previous section, particles produced at pH=4 use to be bigger and the dispersion is higher. This must be considered as a detriment of the size control, and consequently pH=7 must be fixed in order to obtain the smallest clusters. However, when the concentration is constant, this parameter can be used to vary the size of the particles, and then it is important to identify possible effects on the structure of the particles.
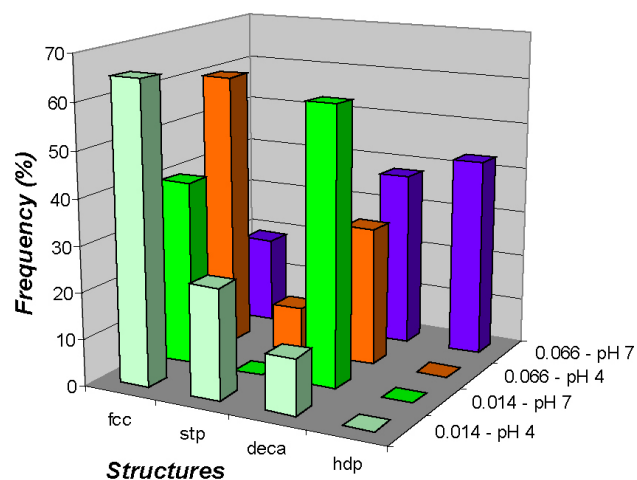
FIGURE 9. Structure distribution plot for the different synthesis conditions.

The structure of the different Au nanoparticles obtained for the compositions with different amounts of the reducing agent was analyzed accurately. For this purpose, the technique of HRTEM has been used to take images with maximum resolution [33].

In Fig. 8 we show representative examples of the nanoparticles found for the different sample preparation conditions, a couple of particles for each synthesis characteristics. While for a concentration of 0.014 mmol and pH=4 the main structures can be associated to fcc-like clusters, as the first ones shown in Fig. 8a with lattice parameters that match with the bulk symmetry of a particle of 6.2 nm diameter, and it is also shown a multiple twin particle, where at least two different disclinations can be identified, this can be associate to the strain fields acting during the pasivation into a single twin cluster [34,35]. For samples obtained with similar concentration but at pH=7, the behavior is different because most of the particles are multiple twinned, with a few fcc-like as in Fig. 8b, where a cubic particle of 3.8 nm diameter is shown besides a 4.8 nm diameter truncated decahedron near to the five-fold orientation.

When the concentration is increased to 0.066 mmol, particles obtained at pH=4 show a preferential formation of fcc-like structures and single twin clusters as it can be seen in Fig. 8c, where a cubic array is associated to the particle with 8 nm diameter; while the second cluster of 7.2 nm diameter, shows a multiple twin structure that can be associated to the decahedral geometry. Besides for the pH=7, particles are mainly decahedrons and small fcc-like as the shown in Fig. 8d, where a decahedron of 4 nm and a cubic cluster of 2.8 nm are shown.

The morphologies of the particles obtained with different pH conditions have been vastly discussed and it has been associated to the competence of active sites during the saturation of the organic reducer and passivation processes [36]. However in our case we also can determine the influence of the amount of metallic salt added and on the reducing agent concentration. For this case, when 0.014 mmol of

$HAuCl_4.xH_2O$ was added with two different amounts of the reducing agent (final pH value of 4 and 7), the morphologies of the particles are totally different. This is illustrated in the Fig. 9. The main structures were: fcc-like type (64%), a smaller quantity of the simple twin particle type (24%) and, finally, the decahedral structures (12%). On the other hand, the Au sample with final pH value of 7, contrary to the previous sample, the main structures were of the decahedral type (60%) and a smaller percentage of the fcc-like type structures (40%).

The influence of concentration and pH is clearly determined in the previous analysis, and the physicochemical processes that induce these tendencies involve the energy reduction of the cluster surface; particularly for a plenty saturation of active sites during the synthesis. In our case we can determine that both parameters involve influence into the generation of the lowest energy configurations, and also in the size control of them.

4. Conclusions

The chemical reduction method allows us to synthesize metal particles with nanometric size distributions. The structural characterizations by HRTEM and the theoretical analysis of stability suggest the tendency to produce multiple twinned Au-Pt particles when the amount of Au is increased. The core-shell system is the more stable. The theoretical analysis by quantum mechanics reveals that the electronic structure of the clusters is significantly affected by the morphological configurations and the elemental distributions, inducing higher catalytic activity for the systems where the Pt atoms are exposed. The size of Au nanoparticles increases as the Au ions in the reaction mixture increases. At low concentrations, decahedra and fcc-deformed structures are the most commonly obtained structures. Higher concentrations induce the formation of single twinned and fcc-like particles. Furthermore, small amounts of the reducing agent induce the formation of fcc-like particles and large amounts of this agent induce the formation of decahedral type of particles.

The synthesis conditions are critical in the size control of the particles, and the use of several combinations of these conditions derive into the possibility to have nanoparticles around 2 nm, and bigger than that. In our studies we can identify the energetic effect of the concentration and the pH conditions for the reduction of metal ions to form small clusters. And the main structures produced in all the case are fcc-like and decahedrons, which have been recognized by multiple authors as the most stable ones.

Acknowledgement

1. M. José-Yacamán, J.A. Ascencio, S. Tehuacanero, and M. Marín, *Top Catal* **18** (2002) 167.

2. X. Li, X. Quan, and C. Kutal, *Scripta Mater.* **50** (2004) 499

3. U. Pal, J.F. Sanchez, S.A. Gamboa, P.J. Sebastian, and R. Pérez, *Phys. Stat. Solid. C* **8** (2003) 2944.

4. A.T. Bell, *Science* **299** (2003) 1688.

5. C. Pan, Z. Zhang, X. Su, Y. Zhao, and J. Liu, *Phys. Rev. B* **70** (2004) 23340.

6. N. Braidy, G.A. Botton, and A. Adronov, *Nanoletters* **2** (2002) 1277.

7. T.S. Kim, W. Sun, C.J. Choi, and B.T. Lee, *Rev. Adv. Mater. Sc.* **5** (2003) 481.

8. Y.Y. Takasu, T. Kawaguchi, W. Sugimoto, and Y. Murakami, *Electrochim. Acta* **48** (2003) 3861.

9. C. Roth, G. Goetz, and H. Fuess, *J. Appl. Electrochem.* **31** (2001) 793.

10. Bin Zhang *et al.*, *Langmuir* **21** (2005) 7449.

11. M.H. Rashid, R.R. Bhattacharjee, A. Kotal, and T.K. Mandal, *Langmuir* **22** (2006) 7141.

12. Shaojun Guo and Erkang Wang, *Analytica Chimica Acta* **598** (2007) 181.

13. Arnim Henglein, *J. Phys. Chem. B* **104** (2000) 2201.

14. A. Zaluska, L. Zaluski, and J.O. Strom-Olsen, *Appl. Phys. A* **72** (2000) 157.

15. J.A. Ascencio, M. Perez, S. Tehuacanero, and M. Jose-Yacamán, *Appl. Phys. A* **73** (2001) 295.

16. H.B. Liu, M. Jose-Yacamán, R. Pérez, and J.A. Ascencio, *Appl. Phys. A* **77** (2003) 63.

17. M. Jose-Yacamán, C. Zorrilla, J.A. Ascencio, G. Mondragón, and J. Reyes-Gasga, *Mat. Trans., JIM*, **40** (1999) 141.

18. L. Beltran del Rio and A. Gomez, *SimulaTEM* (1999)

19. A. Gomez, *Micros. Res. Technol.* **40** (1998) 37.

20. *DMol3 module of Cerius2 by Accelrys*, (San Diego 1999)

21. J. Perdew and Y. Wang, *Phys. Rev. B* **45** (1992) 13244.

22. K.B. Male, J.J. Li, C.C. Bun, S.C. Ng, and J.H.T. Luong, *J. Phys. Chem. C.* **112** (2008) 443.

23. D. Nagao, Y. Shimazaki, Y. Kobayashi, and M. Konno, *Coll. Surf. A-Physicochem. Eng. Aspects.* **273** (2006) 97.

24. H. Assaoudi *et al.*, *Nanotechnology* **18** (2007) 445606.

25. V. Johanek *et al.*, *Science* **304** (2004) 1639.

26. J.A. Ascencio, M. Pérez, and M. José-Yacamán, *Surf. Sci.* **447** (2000) 73.

27. J.A. Ascencio *et al.*, *Surf. Sci.* **396** (1998) 349.

28. R. Esparza *et al.*, *J. Nanosci. Nanotechno.* **5** (2005) 641.

29. R. Faridi-Majidi and N. Sharifi-Sanjani, *J. Magn. Magn. Mat.* **311** (2007) 55.

30. S. Velumani, J.A. Ascencio, U. Pal, G. Canizal, and P.J. Sebastian, *J. Pol. Sci. B: Pol. Phys.* **43** (2005) 3058.

31. H.B. Liu, J.A. Ascencio, M. Perez, and M. Jose-Yacaman, *Surf. Sci.* **491** (2001) 88.

32. J.A. Ascencio, Y. Mejia, H.B. Liu, C. Angeles, and G. Canizal, *Langmuir* **19** (2003) 5882.

33. Y. Lei and W.K. Chim, *J. Am. Chem. Soc.* **127** (2005) 1487.

34. J.A. Ascencio *et al.*, *J. Clus. Sci.* **13** (2002) 189.

35. H.B. Liu, U. Pal, R. Perez, and J.A. Ascencio, *J. Phys. Chem. B* **110** (2006) 5191.

36. R. Esparza, G. Rosas, M. López-Fuentes, U. Pal, and R. Pérez, *Rev. Mex. Fís.* **53** (2007) 67.